Enhanced MIMO LMMSE Turbo Equalization: Algorithm, Simulations, and Undersea Experimental Results

Jun Tao, *Member, IEEE*, Jingxian Wu, *Member, IEEE*, Yahong Rosa Zheng, *Senior Member, IEEE*, and Chengshan Xiao, *Fellow, IEEE*

***Abstract*—In this paper, an enhanced linear minimum mean square error (LMMSE) turbo equalization scheme is proposed for multiple-input multiple-output (MIMO) communication systems with bit-interleaved coded modulation (BICM) in the time domain and multiplexing in the space domain. The proposed turbo equalization scheme outperforms the conventional LMMSE turbo equalization by adopting two new signal processing techniques. First, it performs hybrid soft interference cancellation (HSOIC) by subtracting the soft decisions of the interfering symbols, and the soft decisions are calculated by using a hybrid of the *a priori* information at the equalizer input and the *a posteriori* information at the equalizer output. Second, it employs a novel block-wise reliability-based ordering scheme such that more "reliable" symbols are detected before the less "reliable" ones to reduce error propagation in HSOIC. The symbol reliability information is based on the symbol *a priori* probability, as a unique byproduct of turbo detection, thus can be obtained with very small overhead. A low-complexity approximation of the enhanced MIMO LMMSE turbo equalization is also proposed to balance the tradeoff between complexity and performance. The performance of the enhanced MIMO LMMSE turbo equalization has been verified through both numerical simulations and the undersea experimental data collected in the SPACE08 experiment launched near Martha's Vineyard, Edgartown, MA, in 2008.**

***Index Terms*—Hybrid soft interference cancellation, reliability-based ordering, turbo equalization, underwater acoustic communication.**

I. Introduction

TURBO equalization improves the performance of communication systems via iterative equalization and decoding between a soft-decision equalizer and a soft-decision channel decoder. Optimum turbo equalization can be achieved by employing the maximum *a posteriori* probability (MAP) algorithms such as the Bahl–Cocke–Jelinek–Raviv (BCJR) algorithm [1], or the maximum-likelihood (ML) algorithms such as the soft-output Viterbi algorithm (SOVA) [2], [3], for the equalizer and the channel decoder. Both SOVA and BCJR algorithms are based on a trellis structure. When used for an equalizer, the computational complexity of the trellis-based algorithms grows exponentially as $S^{N(L-1)}$[4], where S, N, and L are the modulation constellation size, the number of transmit antennas, and the channel length, respectively. In many practical scenarios like underwater acoustic communication, where the channel length L amounts to the order of hundreds [5], the complexity of the optimum turbo equalization becomes prohibitively high, and this makes trellis-based equalization algorithms infeasible.

Suboptimal turbo equalization with much lower complexity than the optimal equalization has attracted extensive attention in the past decade [6]–[20]. In [6]–[12], linear minimum mean-square error (LMMSE) filtering combined with soft interference cancellation (SOIC) has been used to replace the BCJR-based optimum equalization for single-input single-output (SISO) systems. The extensions of LMMSE turbo equalization to multiple-input multiple-output (MIMO) systems are found in [13], [14]. Separate time equalization and space equalization is proposed in [14] to generate more degrees of freedom in the equalizer design. In [15], pre-filtering is employed to reduce the number of channel trellis states so that the BCJR-based equalization can be performed with reduced complexity for MIMO systems. Iterative decision-feedback equalizer (DFE) has also been proposed in [16]–[18] for suboptimal turbo equalization. In [18], the iterative DFE has been applied to MIMO underwater acoustic communication using both space-time trellis codes (STTCs) and layered space-time codes (LSTCs). Motivated by [21], [22], iterative block decision feedback equalizer (BDFE) has also been proposed in [19] and [20] for SISO and MIMO systems, respectively.

Most existing suboptimal turbo equalization algorithms employ SOIC to balance the complexity-performance tradeoff. In the linear turbo equalization [6]–[12], the SOIC is performed with the *a priori* soft information calculated from the log-likelihood ratio (LLR) at the input of the equalizer, and we denote it as the *a priori* soft decision in this paper. In decision-feedback turbo equalization [16]–[20], the soft decision of an equalized symbol is fed back and canceled during the detection of the remaining symbols, and it is denoted as the *a posteriori* soft

Manuscript received October 13, 2010; revised February 06, 2011; accepted April 08, 2011. Date of publication April 29, 2011; date of current version July 13, 2011. The associate editor coordinating the review of this manuscript and approving it for publication was Prof. Xiqi Gao. Part of the material in this paper was presented at the IEEE Vehicular Technology Conference (VTC), Ottawa, Canada, September 2010. The work was supported in part by NSF under Grants ECCS-0846486, CCF-0915846, and ECCS-0917041, and by the Office of Naval Research under Grants N00014-09-1-0011 and N00014-10-1-0174.

J. Tao, Y. R. Zheng, and C. Xiao are with the Department of Electrical and Computer Engineering, Missouri University of Science & Technology, Rolla, MO 65409 USA (e-mail: jtb84@mail.missouri.edu; zhengyr@mst.edu; xiaoc@mst.edu).

J. Wu is with the Department of Electrical Engineering, University of Arkansas, Fayetteville, AR 72701 USA (e-mail: wuj@uark.edu).

Color versions of one or more of the figures in this paper are available online at http://ieeexplore.ieee.org.

Digital Object Identifier 10.1109/TSP.2011.2147782

decision in this paper. In [23], a sequential iterative linear estimation scheme is proposed for SISO orthogonal frequency-division multiplexing (OFDM) systems, where the outcomes of previously estimated symbols are incorporated into the estimation of subsequent symbols. This iterative scheme does not include the channel decoding, thus it is not a turbo equalization in the strict sense. However, it indicates an improved SOIC mechanism, since the so-called outcome of a previously estimated symbol is equivalent to the *a posteriori* soft decision, which is usually more reliable than the *a priori* soft decision attributing to the extra information gleaned in the estimation process.

In this paper, we propose an enhanced LMMSE turbo equalization scheme for a MIMO system with bit-interleaved coded modulation (BICM) in the time domain and multiplexing in the space domain. Compared with existing schemes, there are two enhancements in the new turbo equalization scheme.

First, the proposed scheme adopts a hybrid SOIC (HSOIC) mechanism, where the interference cancellation is performed by using both the *a priori* soft decisions at the equalizer input and the *a posteriori* soft decisions at the equalizer output. Due to the relatively higher quality of the *a posteriori* soft decisions, the combination of the *a priori* and the *a posteriori* soft decisions yields a better performance compared to the conventional SOIC used in [6]–[12]. At the mean time, the HSOIC incurs a very small overhead compared to the conventional SOIC, because the *a posteriori* soft decision can be efficiently calculated based on the equalized symbols. Moreover, compared with DFE [16] or generalized DFE (GDFE) [22], where the *a posteriori* decisions are assumed to be error free in the equalizer design, the enhanced LMMSE turbo equalization does not require any assumption on the *a posteriori* soft decisions.

Second, we propose a novel *block-wise, reliability-based* detection ordering scheme, where symbols are grouped into blocks in the fashion that those severely interfering each other are in the same block, and within each block, symbols with higher *a priori* reliability will be equalized before those with lower *a priori* reliability. The detection ordering is critical to the HSOIC because the *a posteriori* soft decision of a given symbol will affect the detection of the subsequent symbols yet to be equalized. In the proposed ordering scheme, the reliability information is extracted from the *a priori* LLR at the equalizer input. Compared with conventional ordered successive interference cancellation (OSIC) schemes [24]–[26], the reliability-based ordering has several unique advantages. First, since the *a priori* LLR is a byproduct of turbo equalization, the proposed ordering can be performed with a very low overhead. On the other hand, conventional OSIC schemes determine the detection order by relying on the channel conditions, and it usually involves intensive computations such as matrix inverse. Second, the proposed scheme performs ordering in a two-dimensional (2-D) time-space domain, while existing OSIC schemes perform ordering only in a one-dimensional (1-D) space domain. In addition, the reliability-based ordering is inherently dynamic as the turbo iterations progress, yet the ordering based on channel conditions in the OSIC scheme remains unchanged throughout the detection process.

In addition to the exact implementation with the equalizer taps updated for each symbol, a low-complexity solution is also provided for the enhanced turbo equalization. Most conventional low-complexity approximations reduce computational complexity by simply using constant equalizer taps for all the symbols [9], [17]. In this paper, we propose a new low-complexity implementation, where the updating of the equalizer taps can be flexibly adjusted to achieve complexity-performance tradeoffs for different applications. The performance gain of the enhanced turbo equalization over its conventional counterpart is verified by numerical simulations with ideal channel knowledge, and by using experimental data measured in underwater acoustic communication experiments with estimated channel conditions. Both simulation and experimental results show that the enhanced turbo equalization consistently outperforms the conventional LMMSE turbo equalization schemes.

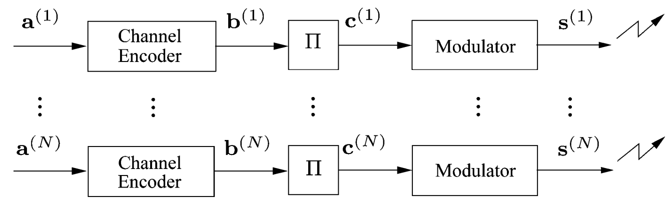

Fig. 1. The transmitter structure of a MIMO system with BICM and spatial multiplexing.

The rest of this paper is organized as follows. In Section II, a MIMO system model with BICM and spatial multiplexing is presented, and the conventional MIMO LMMSE turbo equalization is briefly reviewed. Section III develops the enhanced MIMO LMMSE turbo equalization, where the HSOIC and the block-wise reliability-based ordering scheme are discussed. In Section IV, a low-complexity solution of the enhanced turbo equalization is provided. Numerical simulations and undersea experimental results are presented in Sections V and VI, respectively. Section VII concludes the paper.

Notation: The superscripts $(\cdot)^t$ and $(\cdot)^h$ represent the matrix transpose and conjugate transpose, respectively. The operators, $\mathbb{E}(\cdot)$ and $\text{cov}(\cdot)$, perform expectation and auto-covariance operations, respectively. The $i \times j$ complex matrix space is represented by $\mathcal{C}^{i\times j}$. An identity matrix of size j is represented as $\mathbf{I}_j$, and a $j \times j$ diagonal matrix with diagonal elements $d_1, d_2, \ldots, d_j$ is denoted as $\text{diag}\{d_1, d_2, \ldots, d_j\}$. The function $\tanh(x)$ denotes hyperbolic tangent.

II. MIMO System Model and Conventional Soft-Decision LMMSE Equalizer

Consider an $N \times M$ MIMO system employing BICM and spatial multiplexing, where N and M are the number of transmit antennas and the number of receive antennas, respectively. The diagram of the transmitter is shown in Fig. 1. From the figure, N bit streams, $\{\mathbf{a}^{(n)}\}_{n=1}^{N}$, are independently encoded, interleaved, and modulated. On the nth branch, the outputs of the encoder, the interleaver (Π), and the modulator are denoted by $\mathbf{b}^{(n)}$, $\mathbf{c}^{(n)}$, and $\mathbf{s}^{(n)}$, respectively. For a 2^Q-ary modulation with the constellation set $\mathcal{S} = \{\chi_i\}_{i=1}^{2^Q}$, every Q coded bits are mapped onto one modulation symbol, i.e., the group of the coded bits, $\{c_{n,k}^q\}_{q=1}^{Q}$, are mapped to the modulation symbol $s_{n,k}$. The modulated symbols on the nth branch are transmitted by the nth transmit antenna in the form of a length-N_p packet as, $\mathbf{s}^{(n)} = [s_{n,1}, \ldots, s_{n,N_p}] \in \mathcal{S}^{1\times N_p}$.

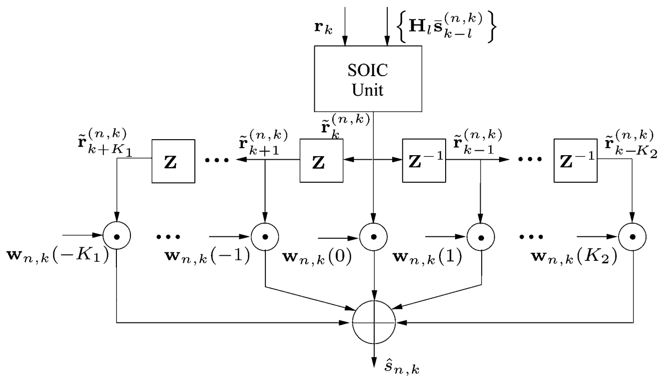

Fig. 2. Tapped-delay-line structure for the estimation of symbol $s_{n,k}$.

The received sample on the mth receive antenna at the time instant k is represented by

$$r_{m,k} = \sum_{l=0}^{L-1}\sum_{n=1}^{N} h_{m,n}(l)s_{n,k-l} + v_{m,k} \tag{1}$$

where $\{h_{m,n}(l)\}_{l=0}^{L-1}$ is the length-L discrete-time channel impulse response (CIR) between the nth transmit antenna and the mth receive antenna, and $v_{m,k}$ is the zero-mean additive white Gaussian noise (AWGN) with variance σ_v^2. Stacking $\{r_{m,k}\}_{m=1}^{M}$ into a column vector, $\mathbf{r}_k = [r_{1,k}, r_{2,k}, \dots, r_{M,k}]^t \in \mathcal{C}^{M\times 1}$, leads to

$$\mathbf{r}_k = \sum_{l=0}^{L-1}\mathbf{H}_l\mathbf{s}_{k-l} + \mathbf{v}_k \tag{2}$$

where

$$\mathbf{H}_l = \begin{bmatrix} h_{1,1}(l) & \cdots & h_{1,N}(l) \\ \vdots & \ddots & \vdots \\ h_{M,1}(l) & \cdots & h_{M,N}(l)\end{bmatrix} \in \mathcal{C}^{M\times N} \tag{3}$$

$$\mathbf{s}_{k-l} = [s_{1,k-l}, s_{2,k-l}, \dots, s_{N,k-l}]^t \in \mathcal{S}^{N\times 1} \tag{4}$$

$$\mathbf{v}_k = [v_{1,k}, v_{2,k}, \dots, v_{M,k}]^t \in \mathcal{C}^{M\times 1}. \tag{5}$$

For a soft-decision linear equalizer, the LMMSE estimation of the symbol $s_{n,k}$ with SOIC is illustrated in Fig. 2. The SOIC is performed over the received signal, $\mathbf{r}_k$, and the output of the SOIC is denoted as $\tilde{\mathbf{r}}_k^{(n,k)} \in \mathcal{C}^{M\times 1}$. The superscript $(\cdot)^{(n,k)}$ indicates that the vector is used for the detection of the kth symbol from the nth transmit antenna. The output of the SOIC is then passed through a tapped-delay-line filter with vector tap $\mathbf{w}_{n,k}(l) \in \mathcal{C}^{M\times 1}$, such that the signals from all the M receive antennas are processed jointly as in [13]. The tap index l goes from $-K_1$ to K_2, which corresponds to a sliding window $[k-K_2, k+K_1]$. The parameters K_1 and K_2 are both positive integers.

The operation of the SOIC and the design of the symbol-wise vector taps, $\{\mathbf{w}_{n,k}(l)\}_{l=-K_1}^{K_2}$, require the *a priori* knowledge of the transmitted symbols. Define, respectively, the *a priori* mean, $\bar{s}_{n,k}$, and the *a priori* variance, $\sigma_{n,k}^2$, of the symbol $s_{n,k}$ as

$$\bar{s}_{n,k} = \sum_{i=1}^{2^Q}\chi_i P(s_{n,k} = \chi_i) \tag{6a}$$

$$\sigma_{n,k}^2 = \sum_{i=1}^{2^Q}|\chi_i - \bar{s}_{n,k}|^2 P(s_{n,k} = \chi_i) \tag{6b}$$

where the symbol *a priori* probability is obtained as $P(s_{n,k} = \chi_i) = \prod_{q=1}^{Q} P\left[c_{n,k}^q = c_i^q\right]$, with the bit sequence $\{c_i^q\}_{q=1}^{Q}$ mapped to the symbol χ_i. The bit *a priori* probability, $P\left[c_{n,k}^q = c_i^q\right]$, is computed from the bit *a priori* LLR, $\Lambda_a(c_{n,k}^q)$, as

$$P\left[c_{n,k}^q = c_i^q\right] = \frac{1 + \dot{c}_i^q \tanh\left(\frac{\Lambda_a(c_{n,k}^q)}{2}\right)}{2} \tag{7}$$

where

$$\dot{c}_i^q = \begin{cases} +1, & c_i^q = 0, \\ -1, & c_i^q = 1. \end{cases} \tag{8}$$

In the first iteration, there is no *a priori* information available thus $\Lambda_a(c_{n,k}^q) = 0$. Starting from the second iteration, $\Lambda_a(c_{n,k}^q)$ at the input to the equalizer is the interleaved output of the soft channel decoder [9]. In the conventional soft-decision LMMSE equalizer [6], the SOIC is performed by subtracting the *a priori* mean of the interfering symbols from $\mathbf{r}_k$ as

$$\tilde{\mathbf{r}}_k^{(n,k)} = \mathbf{r}_k - \sum_{l=0}^{L-1}\mathbf{H}_l\bar{\mathbf{s}}_{k-l}^{(n,k)} \tag{9}$$

where $\bar{\mathbf{s}}_j^{(n,k)} = [\bar{s}_{1,j}, \dots, \bar{s}_{N,j}]^t$ when $j \neq k$, and $\bar{\mathbf{s}}_j^{(n,k)} = [\bar{s}_{1,j}, \dots, \bar{s}_{n-1,j}, 0, \bar{s}_{n+1,j}, \dots, \bar{s}_{N,j}]^t$ when $j = k$. The estimated symbol at the output of the tapped-delay-line filter is given as

$$\hat{s}_{n,k} = \sum_{l=-K_1}^{K_2}\mathbf{w}_{n,k}^h(l)\tilde{\mathbf{r}}_{k-l}^{(n,k)}. \tag{10}$$

To facilitate the filter design, define the received sample vector over the sliding window as

$$\begin{aligned}\mathbf{y}_k &\triangleq \left[\mathbf{r}_{k-K_2}^t, \mathbf{r}_{k-K_2+1}^t, \dots, \mathbf{r}_{k+K_1}^t\right]^t \in \mathcal{C}^{M(K_1+K_2+1)\times 1} \\ &= \mathbf{H}\mathbf{x}_k + \mathbf{z}_k \end{aligned} \tag{11}$$

where $\mathbf{H} \in \mathcal{C}^{M(K_1+K_2+1)\times N(K_1+K_2+L)}$ is defined as

$$\mathbf{H} \triangleq \begin{bmatrix} \mathbf{H}_{L-1} & \cdots & \mathbf{H}_0 & \mathbf{0} \\ \vdots & \ddots & \ddots & \vdots \\ \mathbf{0} & \mathbf{H}_{L-1} & \cdots & \mathbf{H}_0 \end{bmatrix} \tag{12}$$

and

$$\mathbf{x}_k \triangleq \left[\mathbf{s}_{k-K_2-L+1}^t, \dots, \mathbf{s}_{k+K_1}^t\right]^t \in \mathcal{S}^{N(K_1+K_2+L)\times 1} \tag{13}$$

$$\mathbf{z}_k \triangleq \left[\mathbf{v}_{k-K_2}^t, \dots, \mathbf{v}_{k+K_1}^t\right]^t \in \mathcal{C}^{M(K_1+K_2+1)\times 1}. \tag{14}$$

With the above definitions, the symbol estimation in (10) can be alternatively expressed by

$$\hat{s}_{n,k} = \mathbf{w}_{n,k}^h\tilde{\mathbf{y}}_k^{(n,k)} \tag{15}$$

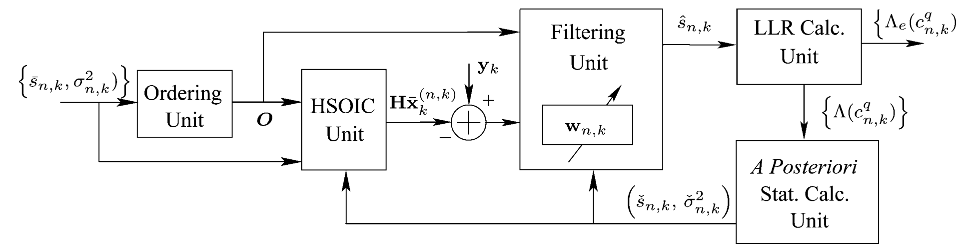

Fig. 3. Block diagram of the enhanced soft-decision MIMO LMMSE equalizer.

where $\mathbf{w}_{n,k} \triangleq [\mathbf{w}^h_{n,k}(K_2), \mathbf{w}^h_{n,k}(K_2-1), \ldots, \mathbf{w}^h_{n,k}(-K_1)]^h \in \mathcal{C}^{M(K_1+K_2+1)\times 1}$ and

$$\tilde{\mathbf{y}}_k^{(n,k)} \triangleq \left[(\tilde{\mathbf{r}}^{(n,k)}_{k-K_2})^t, (\tilde{\mathbf{r}}^{(n,k)}_{k-K_2+1})^t, \ldots, (\tilde{\mathbf{r}}^{(n,k)}_{k+K_1})^t\right]^t = \mathbf{y}_k - \mathbf{H}\bar{\mathbf{x}}_k^{(n,k)} \quad (16)$$

with $\bar{\mathbf{x}}_k^{(n,k)} \in \mathcal{C}^{N(K_1+K_2+L)\times 1}$ defined as

$$\bar{\mathbf{x}}_k^{(n,k)} \triangleq \left[(\bar{\mathbf{s}}^{(n,k)}_{k-K_2-L+1})^t, \ldots, (\bar{\mathbf{s}}^{(n,k)}_{k+K_1})^t\right]^t. \quad (17)$$

The equalizer vector that minimizes the mean square error (MSE), $\mathbb{E}\left[|\hat{s}_{n,k} - s_{n,k}|^2\right]$, is designed as

$$\begin{aligned}\mathbf{w}_{n,k} &= \mathbb{E}[|s_{n,k}|^2]\left\{\mathbf{\Sigma}_k + \left[\mathbb{E}(|s_{n,k}|^2) - \sigma^2_{n,k}\right]\mathbf{h}_n\mathbf{h}_n^h\right\}^{-1}\mathbf{h}_n \\ &= (\sigma^2_{n,k} + \bar{s}^2_{n,k})\left\{\mathbf{\Sigma}_k + \bar{s}^2_{n,k}\mathbf{h}_n\mathbf{h}_n^h\right\}^{-1}\mathbf{h}_n \end{aligned} \quad (18)$$

where $\mathbf{h}_n$ is the $[N(K_2 + L - 1) + n]$th column of $\mathbf{H}$, and $\mathbf{\Sigma}_k \triangleq \mathrm{cov}[\mathbf{y}_k, \mathbf{y}_k] = \mathbf{H}\mathbf{D}_k\mathbf{H}^h + \sigma^2_v\mathbf{I}_{M(K_1+K_2+1)}$ with $\mathbf{D}_k = \mathrm{diag}\{\sigma^2_{1,k-K_2-L+1}, \ldots, \sigma^2_{N,k-K_2-L+1}, |\cdots|, \sigma^2_{1,k+K_1}, \ldots, \sigma^2_{N,k+K_1}\}$. For normalized constant-modulus modulations like phase-shift keying (PSK), the power of the modulation symbol is a constant $\mathbb{E}[|s_{n,k}|^2] = 1$, then the equalizer vector can be simplified to $\mathbf{w}_{n,k} = [\mathbf{\Sigma}_k + (1 - \sigma^2_{n,k})\mathbf{h}_n\mathbf{h}_n^h]^{-1}\mathbf{h}_n$.

In turbo equalization, the equalized symbol $\hat{s}_{n,k}$ will be translated into soft information in the form of extrinsic LLR $\{\Lambda_e(c^q_{n,k})\}$, which is then delivered as the input to the soft-decision channel decoder. The computation of the extrinsic LLR will be described in the next section. The channel decoder generates new extrinsic information, which is fed back to the equalizer to launch the next iteration. In this work, we focus on the enhanced design of the soft-decision equalizer, and details on the turbo equalization are referred to [6].

III. Enhanced Soft-Decision MIMO LMMSE Equalizer

The block diagram of the enhanced soft-decision MIMO LMMSE equalizer is shown in Fig. 3. The HSOIC and the reliability-based ordering scheme are discussed in the next two subsections.

A. HSOIC Scheme

The performance of SOIC depends heavily on the quality of the soft decision. In conventional SOIC, the *a priori* soft decisions of the interfering symbols are subtracted, as indicated in (9). Intuitively, the *a posteriori* soft decision at the output of the equalizer has a better fidelity than the *a priori* soft decision at the input, due to the extra information gleaned in the equalization process. A natural idea is to incorporate the *a posteriori* soft decision into the equalization process.

Since the equalization is performed on a symbol-by-symbol basis, the *a posteriori* soft decision of an already equalized symbols can replace its *a priori* counterpart, and it can be used during the SOIC for the subsequent symbols to be equalized. In this way, the SOIC combines both the *a priori* soft decision (for unequalized symbols) and the *a posteriori* soft decision (for equalized symbols), and we denote the new SOIC scheme as HSOIC. It is expected that extra performance gain can be achieved with HSOIC given the better reliability of the *a posteriori* soft decision. The computation of the *a posteriori* soft decision is next discussed. Based on the equalized symbol $\hat{s}_{n,k}$ at the output of the equalizer, the symbol *a posteriori* probability is expressed as

$$P(s_{n,k} = \chi_i|\hat{s}_{n,k}) = \frac{p(\hat{s}_{n,k}|s_{n,k} = \chi_i)P(s_{n,k} = \chi_i)}{p(\hat{s}_{n,k})} \quad (19)$$

where $P(s_{n,k} = \chi_i)$ is the *a priori* probability, and $p(\hat{s}_{n,k})$ can be obtained by using $\sum_{i=1}^{2^Q} p(s_{n,k} = \chi_i|\hat{s}_{n,k}) = 1$. It is assumed that $\hat{s}_{n,k}$ conditioned on $s_{n,k} = \chi_i$ follows a Gaussian distribution as in [6] and [9]. The conditional mean, $\mu^i_{n,k} \triangleq \mathbb{E}[\hat{s}_{n,k}|s_{n,k} = \chi_i]$, and the conditional variance, $\delta^i_{n,k} \triangleq \mathrm{cov}(\hat{s}_{n,k}, \hat{s}_{n,k}|s_{n,k} = \chi_i)$, can be computed as follows

$$\mu^i_{n,k} = \mathbb{E}[\mathbf{w}^h_{n,k}\tilde{\mathbf{y}}_k^{(n,k)}|s_{n,k} = \chi_i] = \chi_i\mathbf{w}^h_{n,k}\mathbf{h}_n \quad (20)$$

and

$$\begin{aligned}\delta^i_{n,k} &= \mathrm{cov}(\mathbf{w}^h_{n,k}\tilde{\mathbf{y}}_k^{(n,k)}, \mathbf{w}^h_{n,k}\tilde{\mathbf{y}}_k^{(n,k)}|s_{n,k} = \chi_i) \\ &= \mathbf{w}^h_{n,k}[\mathbf{\Sigma}_k - \sigma^2_{n,k}\mathbf{h}_n\mathbf{h}_n^h]\mathbf{w}_{n,k}\end{aligned} \quad (21)$$

where the two identities $\mathrm{cov}(\mathbf{a}^h\mathbf{x}, \mathbf{a}^h\mathbf{x}) = \mathbf{a}^h\mathrm{cov}(\mathbf{x}, \mathbf{x})\mathbf{a}$ and $\mathrm{cov}(\mathbf{x} + \mathbf{a}, \mathbf{x} + \mathbf{a}) = \mathrm{cov}(\mathbf{x}, \mathbf{x})$ are used to obtain (21). The conditional PDF $p(\hat{s}_{n,k}|s_{n,k} = \chi_i)$ is then given as

$$p(\hat{s}_{n,k}|s_{n,k} = \chi_i) = \frac{1}{\pi\delta^i_{n,k}}\exp\left\{-\frac{|\hat{s}_{n,k} - \mu^i_{n,k}|^2}{\delta^i_{n,k}}\right\}. \quad (22)$$

With the *a posteriori* probability given in (19), the *a posteriori* mean and variance of the symbol $s_{n,k}$ can be calculated, respectively, as

$$\check{s}_{n,k} = \sum_{i=1}^{2^Q}\chi_i P(s_{n,k} = \chi_i|\hat{s}_{n,k}) \quad (23a)$$

$$\check{\sigma}^2_{n,k} = \sum_{i=1}^{2^Q}|\chi_i - \check{s}_{n,k}|^2 P(s_{n,k} = \chi_i|\hat{s}_{n,k}). \quad (23b)$$

We propose to use the *a posteriori* mean given in (23a) as the *a posteriori* soft decision. The more reliable *a posteriori* soft decision, $\check{s}_{n,k}$, will then replace the *a priori* soft decision, $\bar{s}_{n,k}$, as the equalization progresses.

Finally, by defining $\varrho^i_{n,k} = \frac{|\hat{s}_{n,k}-\mu^i_{n,k}|^2}{\delta^i_{n,k}}$, the extrinsic bit LLRs corresponding to the symbol $s_{n,k}$ is computed as

$$\Lambda_e(c^q_{n,k}) = \ln \frac{\sum\limits_{\forall \chi_i : c^q_i = 0} \exp\left[-\varrho^i_{n,k} + \frac{1}{2}\sum\limits_{\forall q' : q' \neq q} \dot{c}^{q'}_i \Lambda_a(c^{q'}_{n,k})\right]}{\sum\limits_{\forall \chi_i : c^q_i = 1} \exp\left[-\varrho^i_{n,k} + \frac{1}{2}\sum\limits_{\forall q' : q' \neq q} \dot{c}^{q'}_i \Lambda_a(c^{q'}_{n,k})\right]} \tag{24}$$

B. Block-Wise Detection Ordering Based on the a priori Reliability Information

In conventional turbo equalization [6]–[13], the order in which the symbols are detected does not affect the SOIC performance, since only the *a priori* statistics as shown in (6) are used during the equalization, and they remain unchanged during an entire packet. With the newly proposed HSOIC scheme, the detection order is critical to the detection performance because the *a posteriori* soft decision of a given symbol will affect the SOIC operation of all the subsequent symbols to be equalized. A high-quality soft decision will positively affect the equalization of the subsequent symbols. Consequently, the detection order becomes a new degree of freedom during the equalizer design. Various detection ordering schemes have been discussed in non-iterative one-time equalizers [24]–[26], where large overhead is incurred to determine the order of detection.

Taking advantage of the iterative mechanism of turbo detection, we propose to determine the detection order by using the *a priori* information at the equalizer input. Define the symbol *a priori* reliability as

$$\rho_{n,k} = \frac{1}{\sigma^2_{n,k}} \tag{25}$$

where $\sigma^2_{n,k}$ is the symbol *a priori* variance given in (6b). This definition of “reliability” is motivated by the fact that a lower *a priori* variance means that the *a priori* soft decision is closer to its true value, thus a higher reliability of the *a priori* soft decision.

The next question is how to determine the detection order over an entire packet based on the reliability measures $\{\rho_{n,k}\}$. An intuitive idea is to sort the reliability measures over the entire packet. Such a global ordering may lead to high sorting complexity especially when the packet size N_p is large. To develop a low-complexity ordering scheme, we take into account two facts. First, the performance of SOIC relies on the quality of soft interference symbols; second, for a given symbol, it mainly interferes adjacent symbols within a time window delineated by the delay spread of the multipath channel. The two facts then motivate a block-wise ordering scheme, which will maximize the advantage of HSOIC and accelerate the convergence of the turbo equalization. The ordering procedure is summarized as follows:

Step 1) Divide the reliability sequence of the entire packet into N_b blocks as

$$\mathcal{B}_1 = \{\boldsymbol{\rho}_1, \ldots, \boldsymbol{\rho}_{L_b}\},\ \mathcal{B}_2 = \{\boldsymbol{\rho}_{L_b+1}, \ldots, \boldsymbol{\rho}_{2L_b}\}, \ldots, \\ \mathcal{B}_{N_b} = \{\boldsymbol{\rho}_{(N_b-1)L_b+1}, \ldots, \boldsymbol{\rho}_{N_bL_b}\} \tag{26}$$

where $\boldsymbol{\rho}_k \triangleq [\rho_{1,k}, \ldots, \rho_{N,k}] \in \mathcal{R}^{1\times N}$ contains the *a priori* reliability of symbols from all the N transmit antennas at time k, and L_b is the block size. It is easy to see that $N_p = N_bL_b$. The block size L_b is selected such that symbols within a given block have significant space-time interference (STI) among each other.

Step 2) Define an index mapping operator $\langle\cdot\rangle$ as

$$\langle\cdot\rangle : (n,k) = \langle j\rangle \ \text{with}\, k = \left\lceil \frac{j}{N} \right\rceil, n = \begin{cases} \mathrm{mod}(j,N) \neq 0 \\ N,\ \text{o.w.} \end{cases} \tag{27}$$

then, within each block, sort $\{\rho_{n,k}\}$ in descending order as

$$\mathcal{B}'_i = [\rho_{\langle O'_{(i-1)NL_b+1}\rangle}, \rho_{\langle O'_{(i-1)NL_b+2}\rangle}, \ldots, \rho_{\langle O'_{iNL_b}\rangle}], \\ \text{for}\ i = 1, 2, \ldots, N_b \tag{28}$$

such that $\rho_{\langle O'_{(i-1)NL_b+1}\rangle} \geq \rho_{\langle O'_{(i-1)NL_b+2}\rangle} \geq \cdots \geq \rho_{\langle O'_{iNL_b}\rangle}$. The ordered index set, $\{O'_{(i-1)NL_b+1}, \ldots, O'_{iNL_b}\}$, is a permutation of the index set $\{(i-1)NL_b+1, \ldots, iNL_b\}$.

Step 3) Assemble the N_b ordered blocks $\{\mathcal{B}'_i\}_{i=1}^{N_b}$ as

$$\boldsymbol{\rho} = [\rho_{\langle O'_1\rangle}, \rho_{\langle O'_{NL_b+1}\rangle}, \ldots, \rho_{\langle O'_{(N_b-1)NL_b+1}\rangle}, |\cdots|, \\ \rho_{\langle O'_{NL_b}\rangle}, \rho_{\langle O'_{2NL_b}\rangle}, \ldots, \rho_{\langle O'_{N_bNL_b}\rangle}]^t. \tag{29}$$

From (29), the overall detection order is determined as

$$\boldsymbol{O} = \{\langle O'_1\rangle, \langle O'_{NL_b+1}\rangle, \ldots, \langle O'_{(N_b-1)NL_b+1}\rangle, |\cdots|, \\ \langle O'_{NL_b}\rangle, \langle O'_{2NL_b}\rangle, \ldots, \langle O'_{N_bNL_b}\rangle\}. \tag{30}$$

To simplify the notation, we represent the order in (30) as

$$\boldsymbol{O} = \{\langle O_1\rangle, \langle O_2\rangle, \ldots, \langle O_{N_b}\rangle, |\cdots|, \langle O_{N_b(NL_b-1)+1}\rangle, \\ \langle O_{N_b(NL_b-1)+2}\rangle, \ldots, \langle O_{N_bNL_b}\rangle\}. \tag{31}$$

The block-wise reliability-based ordering scheme is illustrated in Fig. 4, where the detection order has been indicated by the red line in the third step.

IV. Low-Complexity Enhanced Soft-Decision MIMO LMMSE Equalizer

The exact implementation of the enhanced soft-decision equalizer requires the equalizer tap vector, $\mathbf{w}_{n,k}$, to be updated for each symbol as shown in (18). The computation of $\mathbf{w}_{n,k}$ involves an inverse of a square matrix of size $M(K_1+K_2+1)$. In highly dispersive channels like underwater acoustic channel, the symbol-spaced channel length L amounts to several tens or even several hundreds, and this makes the computation complexity prohibitively high. Therefore, it is desirable to provide a low-complexity solution.

We propose a new low-complexity implementation of the enhanced soft-decision equalizer. Most conventional low-complexity implementations reduce the computation complexity by replacing the exact symbol-wise equalization tap vectors with a set of constant tap vectors, which are used for the equalization of the entire packet of symbols. To achieve a flexible complexity-performance tradeoff, we propose to periodically

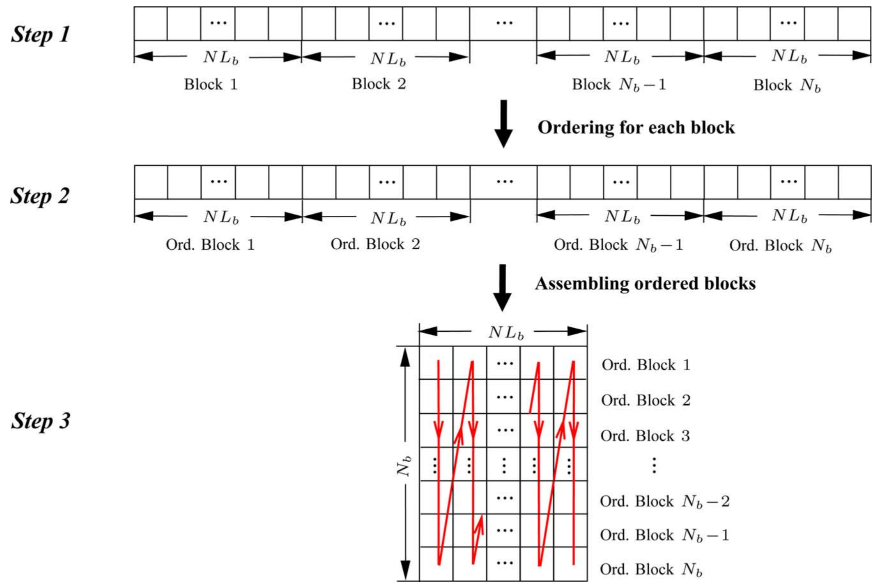

Fig. 4. Block-wise reliability-based ordering scheme (each square in the figure denotes a reliability measure, and the ordering is obtained by collecting the indexes of the reliability measures in the order indicated by the red line as shown in Step 3).

update the equalization tap vectors for every N_b symbols, i.e., a constant set of tap vectors will be used for the equalization of N_b symbols, and the tap vectors will be updated for the next N_b symbols. Details of the new low-complexity implementation are described as follows. Before the equalization starts, a set of low-complexity equalizer tap vectors are first computed as follows

$$\mathbf{w}_n = \left\{\sum_{k=1}^{N_p} \frac{\sigma_{n,k}^2 + \bar{s}_{n,k}^2}{N_p}\right\}\left\{\sum_{k=1}^{N_p} \frac{\mathbf{\Sigma}_k + \bar{s}_{n,k}^2 \mathbf{h}_n \mathbf{h}_n^h}{N_p}\right\}^{-1}\mathbf{h}_n$$
$$= (\bar{\sigma}_n^2 + \bar{\mu}_n^2)(\bar{\mathbf{\Sigma}} + \bar{\mu}_n^2 \mathbf{h}_n \mathbf{h}_n^h)^{-1}\mathbf{h}_n \tag{32}$$

for $n = 1, 2, \ldots, N$, where $\bar{\mathbf{\Sigma}} = \frac{1}{N_p}\sum_{k=1}^{N_p} \mathbf{\Sigma}_k$, $\bar{\mu}_n^2 = \frac{1}{N_p}\sum_{k=1}^{N_p} \bar{s}_{n,k}^2$ and $\bar{\sigma}_n^2 = \frac{1}{N_p}\sum_{k=1}^{N_p} \sigma_{n,k}^2$. The initial equalization vector is used for the detection of N_b symbols, with their indexes indicated by the first column of the array shown in Step 3 of Fig. 4. Once the N_b symbols are equalized, the obtained *a posteriori* soft decisions will be used to update the equalization tap vectors as described in (32), and to replace their *a priori* counterparts for the HSOIC operation during the equalization of the next N_b symbols (with their indexes indicated by the second column of the array shown in the Step 3 of Fig. 4). This above procedure is repeated until all the symbols in a packet are equalized.

We provide two remarks for the periodic equalizer tap updating mechanism.

Remark 1: Each column of the array in Fig. 4 can be considered as a "generalized layer" in the sense that its corresponding symbol indexes scatter over a 2-D space-time domain with their positions determined by the ordering. From the figure, there are $N_L = NL_b$ layers in total. Due to the ordering, the more reliable layer is detected earlier, so that the less reliable layers can take advantage of the improved SOIC.

Remark 2: The complexity for updating the equalizer tap is determined by the number of layers N_L, or equivalently L_b, for a given system. To meet the aforementioned requirement that symbols within a block interfere each other, we set $L_b \leq L$. Under this constraint, the parameter L_b can be flexibly selected so the updating complexity is controllable. It will be shown by both the numerical simulations and experimental results that a small value of L_b captures most of the performance gain, even the underlying channel length L is large. When $L_b = 1$ (the only choice in the special case of flat fading), the number of layers is equal to the number of transmission streams N. The matrix $\bar{\mathbf{\Sigma}}$ in (32) can also be replaced by

$$\tilde{\mathbf{\Sigma}} = \mathbf{H}\mathrm{diag}\{\bar{\sigma}_1^2, \ldots, \bar{\sigma}_N^2, |\cdots|\bar{\sigma}_1^2, \ldots, \bar{\sigma}_N^2\}\mathbf{H}^h + \sigma_v^2\mathbf{I} \tag{33}$$

which leads to an alternative low-complexity solution for the enhanced soft-decision equalizer.

The low-complexity solution of the enhanced soft-decision MIMO LMMSE equalization is summarized in Table I.

V. Simulation Results

Simulation results are presented in this section to demonstrate the performance of the proposed MIMO LMMSE turbo equalization scheme.

Fig. 5 compares the performance between the original and the enhanced MIMO LMMSE turbo equalization. A 2×2 MIMO system with 16QAM modulation is investigated. A rate-$\frac{1}{2}$ non-systematic convolutional channel encoder with generator polynomial $[G_1, G_2] = [17, 13]_{\mathrm{oct}}$ is used. Each subchannel of the 2×2 MIMO system has a uniform power delay profile (PDP) with channel length $L = 10$. The data is transmitted in packets, as mentioned before. Each packet carries $N_p = 1{,}000$ 16QAM symbols. The channel is constant within one packet while changes across packets. The equalizer parameters K_1 and K_2 are set as $K_1 = K_2 = L$. The ordering block size has been chosen as $L_b = 2$ for the enhanced equalization. From the figure, the enhanced equalization achieves a performance gain of 1.5 dB at the BER level 10^{-3} after four

TABLE I
LOW-COMPLEXITY ENHANCED MIMO LMMSE EQUALIZATION ALGORITHM

INPUT:
- Received vector sequence $\{\mathbf{r}_k\}$ of the entire packet;
- Bit *a priori* LLR sequence $\{\Lambda_a(c^q_{n,k})\}$ of the entire packet.

INITIALIZATION:
- Compute the symbol *a priori* mean and variance of the entire packet, $\mathcal{M} = \{\bar{s}_{n,k}\}$ and $\mathcal{V} = \{\sigma^2_{n,k}\}$, according to (6a) and (6b);
- Compute $\mathcal{R} = \{\bar{\mathbf{r}}_k = \sum_{l=0}^{L-1} \mathbf{H}_l \bar{\mathbf{s}}_{k-l}\}$ with $\bar{\mathbf{s}}_k = [\bar{s}_{1,k}, \cdots, \bar{s}_{N,k}]^t$;
- Following the procedure in (26)–(31), to obtain the ordering $\boldsymbol{O}$.

LOW-COMPLEXITY EQUALIZATION ALGORITHM:

FOR $n_l = 1$ TO N_L
- Compute $\{\mathbf{w}_n\}_{n=1}^N$ as in (32), and $\{\beta_n = \mathbf{w}_n^h \mathbf{h}_n\}_{n=1}^N$;

FOR $n_b = 1$ TO N_b
- Obtain $(n_j, k_j) = \langle O_j \rangle$, where $j = (n_l - 1)N_b + n_b$;
- Compute $\hat{s}_{n_j,k_j} = \mathbf{w}_{n_j}^h(\mathbf{y}_{k_j} - \bar{\mathbf{y}}_{k_j}) + \bar{s}_{n_j,k_j}\beta_{n_j}$;

FOR $i = 1$ TO 2^Q
- Compute $\varrho^i_{n_j,k_j} = \frac{\left|\hat{s}_{n_j,k_j} - \mu^i_{n_j,k_j}\right|^2}{\delta^i_{n_j,k_j}}$ with $\mu^i_{n_j,k_j} = \chi_i \beta_{n_j}$ and $\delta^i_{n_j,k_j} = \mathbf{w}_{n_j}^h \boldsymbol{\Sigma}_{k_j} \mathbf{w}_{n_j} - \sigma^2_{n_j,k_j}|\beta_{n_j}|^2$;

END
- For $1 \le q \le Q$, compute $\Lambda_e(c^q_{n_j,k_j})$ according to (24);
- Determine $P(s_{n,k} = \chi_i | \hat{s}_{n,k})$ according to (19)–(22);
- Compute $\check{s}_{n_j,k_j}$ and $\check{\sigma}^2_{n_j,k_j}$ according to (23a) and (23b);
- Update $\bar{s}_{n_j,k_j} \in \mathcal{M}$ with $\check{s}_{n_j,k_j}$, $\bar{\sigma}^2_{n_j,k_j} \in \mathcal{V}$ with $\check{\sigma}^2_{n_j,k_j}$, and corresponding $\bar{\mathbf{r}}$'s in $\mathcal{R}$.

END

END

OUTPUT:
- Extrinsic bit LLRs $\left\{\Lambda_e(c^q_{n,k})\right\}$ of the entire packet.

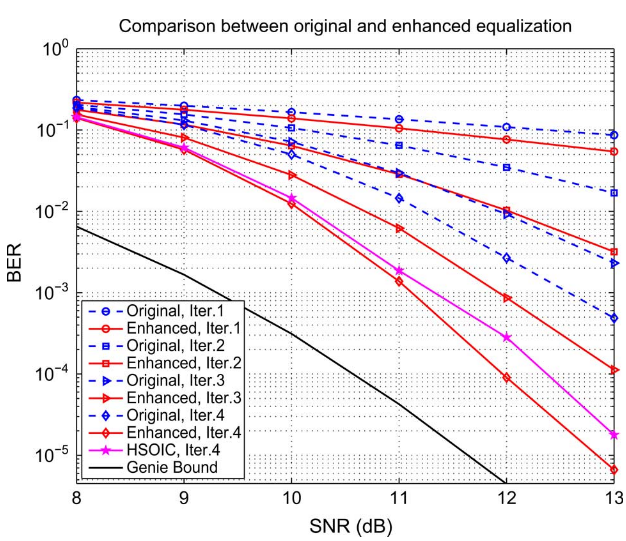

Fig. 5. Performance comparison between the exact implementations of the original and the enhanced MIMO LMMSE turbo equalization (2×2 MIMO, 16QAM, Uniform PDP, $L = 10$).

iterations. In the first iteration, there is no reliability information available for ordering, while extra performance gain is still achieved by the proposed equalization due to the incorporation of the *a posteriori* soft decisions. The simulation result for the equalization using HSOIC without the reliability-based ordering is also included. As expected, the performance of the HSOIC equalization is better than that of the original equalization while is not as good as that of the enhanced equalization.

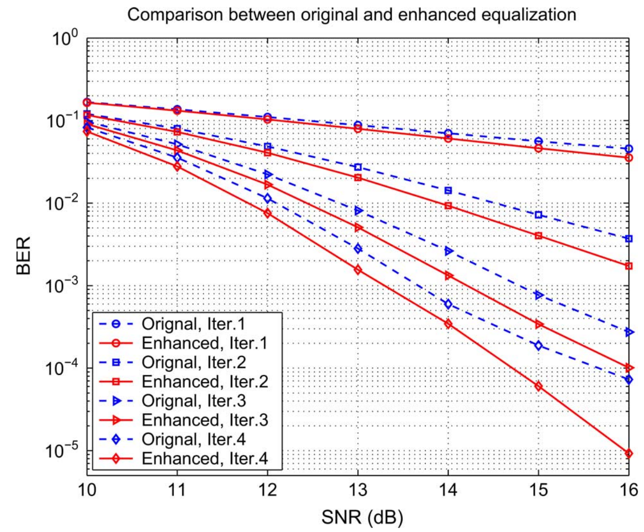

Fig. 6. Performance comparison between the low-complexity implementations of the original and the enhanced MIMO LMMSE turbo equalization (2×2 MIMO, 16QAM, Uniform PDP, $L = 10$).

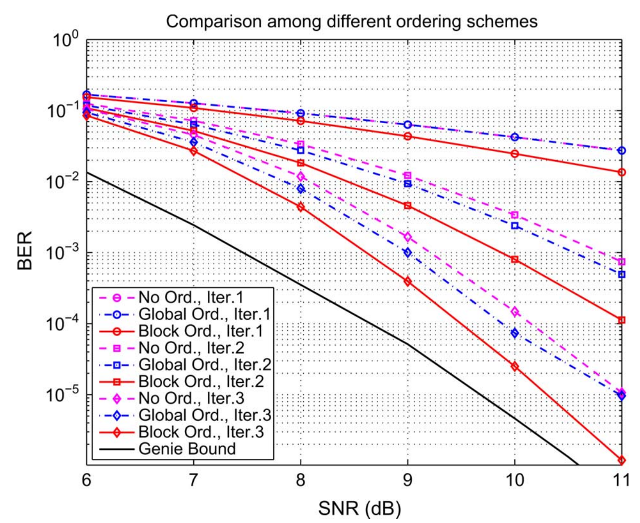

Fig. 7. Performance comparison among different detection ordering schemes (4×4 MIMO, 8PSK, Exponential PDP, $L = 5$, low-complexity implementation).

Not including the reliability-based ordering in the HSOIC leads to a 0.4 dB performance penalty at the BER lever of 10^{-4} at the fourth iteration. The genie lower bound [14] is plotted as a performance benchmark. At BER of 10^{-5}, the performance of the enhanced equalization is 1 dB away from the genie bound.

With other simulation parameters unchanged, the performance comparison between the low-complexity implementations of the original and the enhanced turbo equalization schemes are shown in Fig. 6. The ordering block size is set as $L_b = 4$ for the enhanced equalization. It can be seen from the figure that the low-complexity enhanced turbo equalization also outperforms the original turbo equalization implemented in a low-complexity style, in all four iterations. Comparing Fig. 6 with Fig. 5, we can see that the complexity reduction is achieved at the cost of degraded performance, as expected.

The impact of detection order on the performance is demonstrated in Fig. 7. Without loss of generality, the low-complexity

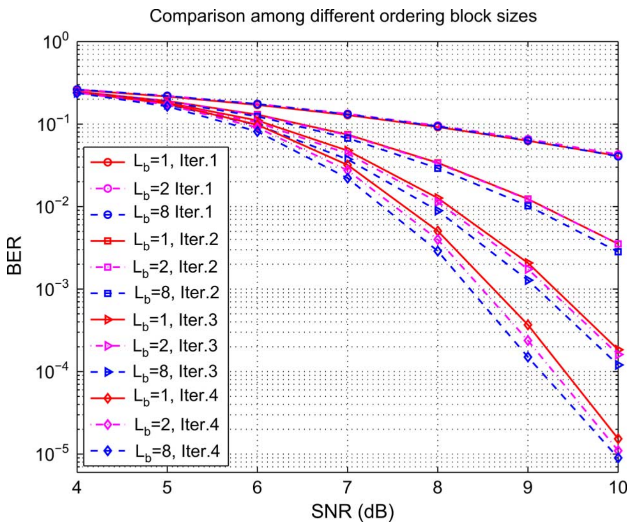

Fig. 8. Performance comparison among different ordering block sizes (2×2 MIMO, 8PSK, Uniform PDP, $L = 10$, low-complexity implementation).

turbo equalization implementations are adopted. The enhanced turbo equalization with no ordering, the global ordering, and the block-wise ordering, are compared. For the global ordering, the ordering is performed over an entire packet. A 4×4 MIMO channel with an exponential PDP and $L = 5$ is adopted. The modulation scheme is 8PSK, and the packet size is $N_p = 1000$. For the block-wise ordering, a block size $L_b = 1$ has been adopted, leading to $N_L = 4$ layers and four times of equalizer tap updating. For comparison fairness, the same number of tap updating has been applied for the other two ordering schemes. From the figure, it is clear that the block-wise ordering leads to the best performance. An interesting observation is that the block-wise ordering achieves extra performance gain, even in the first iteration when no *a priori* reliability information is available. This attributes to its clustering operation (Step 1 in Fig. 4) and assembling operation (Step 3 in Fig. 4), which lead to more effective HSOIC. The global ordering scheme slightly outperforms the non-ordering scheme since the second iteration, and they have the same performance at the first iteration due to the lack of the *a priori* reliability information. At BER = 10^{-5}, the performance of the enhanced equalization with three iterations is only 0.4 dB away from the genie bound.

In Fig. 8, the effect of the ordering block size, L_b, on the detection performance is demonstrated, with the low-complexity turbo equalization implementation. A 2×2 MIMO channel with a uniform PDP and $L = 10$ is used. The modulation scheme is 8PSK and the packet size is $N_p = 1000$. Under the constraint $L_b \leq L$ such that symbols within each block interfere each other, three block sizes $L_b = 1$, $L_b = 2$ and $L_b = 8$ are investigated, corresponding to 2, 4, and 16 times of equalizer tap updating. From the figure, a choice of $L_b = 1$ achieves similar performance as $L_b > 1$, at a considerably reduced complexity.

VI. Undersea Experimental Results

The enhanced MIMO LMMSE turbo equalization has been adopted to process experimental data measured in the SPACE08 underwater acoustic communication experiment, which was conducted off the coast of Martha's Vineyard, Edgartown, MA, in October 2008. In this experiment, the symbol interval was $T_s = 0.1024$ ms and the carrier frequency was $f_c = 13$ kHz. The transmission equipment consisted of four transducers, and the receiver had twelve hydrophones. The communication distance ranged from 60 to 1000 m. During the experiment, the number of active transducers could be configured to launch different MIMO transmissions. A packet transmission scheme was adopted, with the packet structure shown in Fig. 9. The packet starts with a *m*-sequence of size 511, which can be used for Doppler estimation and compensation if necessary [5]. The data payload consists of multiple frames of size N_F, and each frame starts with a length-N_T pilot block followed by multiple length-N_B information blocks. To adapt to the time variation of the underwater acoustic channel, the N_T previously-detected symbols are also used to re-estimate the channel for detecting the current block.

Fig. 10 shows an example of the estimated underwater acoustic channel, where "T" and "H" denote a transducer and a hydrophone, respectively. It is obvious all subchannels are sparse and the channel length is as long as $L = 100$. Except the T2-H2 subchannel, the other three are non-minimum phase. Such a MIMO channel makes the channel equalization very challenging.

The low-complexity algorithms of the original and enhanced equalization methods are applied to the detection of real-world data. For the enhanced equalization, a block size of $L_b = 1$ thus $N_b = N_p$ is adopted for the ordering. In this case, the equalizer tap is updated $N_L = N$ times during the detection of each packet.

In Table II, the detection result for a 200-m two-transducer MIMO transmission with QPSK modulation is presented. The packet parameters are $N_B = 300$, $N_T = 600$ and $N_F = 6{,}000$ corresponding to a pilot overhead of 10%. Four hydrophones with indexes 1, 5, 9, 12 are used during the detection. From the table, it is clear that the enhanced equalizer consistently outperforms the original equalizer for all eight packets. The average number of errors listed in the last row shows that at the third iteration, the enhanced equalizer achieves a BER that is about $1 \sim 2$ order of magnitudes lower than that of the original equalizer.

The result for a 1000-m two-transducer MIMO transmission with 8PSK modulation is listed in Table III. The packet parameters are $N_B = 300$, $N_T = 600$, and $N_F = 3000$ incurring 20% pilot overhead. Six hydrophones with odd indexes have been chosen for the detection. The enhanced turbo equalizer again manifests better performance than the original turbo equalizer.

In Table IV, the detection result for a three-transducer MIMO transmission is demonstrated, where the first four packets were measured at a transmission range of 200 m, and the last six ones were measured during a 1000-m transmission. The packet parameters are $N_B = 200$, $N_T = 600$ and $N_F = 2400$ (except the last frame whose size is $N_F = 1200$). The pilot overhead is 26%. All twelve hydrophones are used for detection to obtain the maximum diversity gain. From the table, significant performance improvement over the original equalization is observed with the enhanced equalization.

An example of processing a packet measured during a 1000-m four-transducer transmission is demonstrated in

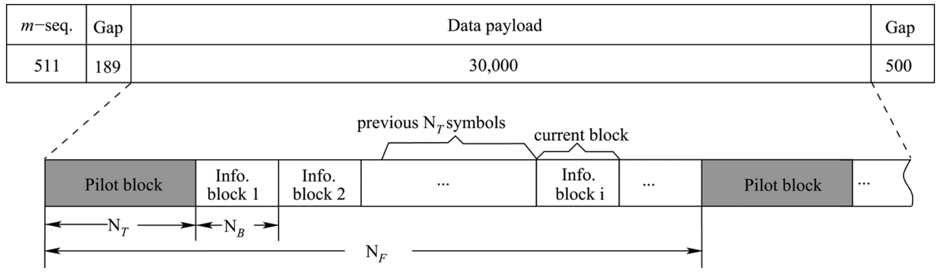

Fig. 9. The packet structure used in the SPACE08 underwater experiment.

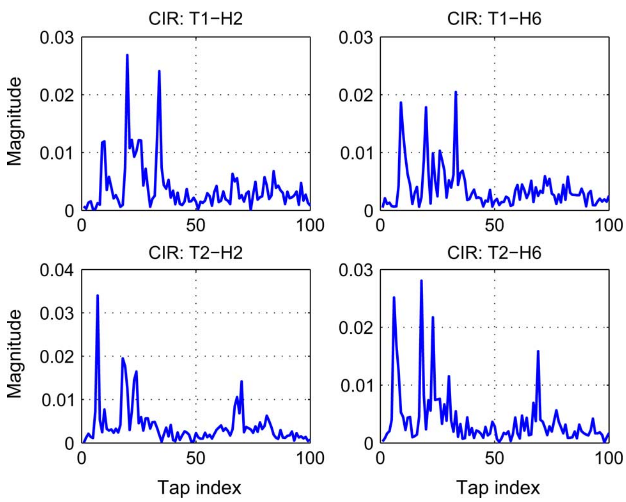

Fig. 10. Impulse response of the estimated underwater acoustic channels (transmission distance is 200 m).

TABLE II
RESULTS FOR 2×4 MIMO (QPSK)

Packet Index	Equ. Algorithm	Err. Num. ($1 \sim 4$ Iter.)
1	Original Enhanced	1062, 0, 0, 0 498, 0, 0, 0
2	Original Enhanced	8485, 92, 0, 0 6740, 12, 0, 0
3	Original Enhanced	2378, 0, 0, 0 1876, 0, 0, 0
4	Original Enhanced	7713, 73, 0, 0 6005, 0, 0, 0
5	Original Enhanced	2048, 0, 0, 0 1440, 0, 0, 0
6	Original Enhanced	16531, 12242, 2112, 0 14804, 6972, 39, 0
7	Original Enhanced	1524, 0, 0, 0 1118, 0, 0, 0
8	Original Enhanced	9585, 209, 0, 0 6328, 17, 0, 0
Average	Original Enhanced	6166, 1577, 264, 0 4851, 875, 5, 0

Table V. The packet parameters are $N_B = 200$, $N_T = 600$, and $N_F = 2000$ corresponding to a pilot overhead of 30%. The error numbers for each of the four transducers are listed. It is apparent that the enhanced equalization considerably improves the detection performance for all four transducers, compared with the original equalization.

TABLE III
RESULTS FOR 2×6 MIMO (8PSK)

Packet Index	Equ. Algorithm	Err. Num. ($1 \sim 4$ Iter.)
1	Original Enhanced	2911, 19, 0, 0 2547, 12, 0, 0
2	Original Enhanced	1584, 5, 0, 0 1367, 0, 0, 0
3	Original Enhanced	4017, 54, 0, 0 2841, 24, 0, 0
4	Original Enhanced	4693, 163, 0, 0 3736, 82, 0, 0
5	Original Enhanced	2235, 18, 0, 0 1788, 14, 0, 0
Average	Original Enhanced	3088, 52, 0, 0 2456, 26, 0, 0

TABLE IV
RESULTS FOR 3×12 MIMO (QPSK)

Packet Index	Equ. Algorithm	Err. Num. ($1 \sim 4$ Iter.)
1	Original Enhanced	15177, 7032, 372, 0 12338, 2930, 6, 0
2	Original Enhanced	11146, 3089, 40, 10 8975, 878, 1, 0
3	Original Enhanced	13093, 3722, 23, 0 10607, 1698, 0, 0
4	Original Enhanced	11436, 4034, 140, 0 10005, 2477, 17, 0
5	Original Enhanced	19227, 12418, 4795, 217 15659, 6623, 479, 0
6	Original Enhanced	7065, 38, 0, 0 3706, 0, 0, 0
7	Original Enhanced	16766, 6293, 164, 0 13935, 2878, 3, 0
8	Original Enhanced	10800, 672, 0, 0 7891, 85, 0, 0
9	Original Enhanced	14119, 2576, 2, 0 9584, 237, 0, 0
10	Original Enhanced	22942, 15380, 7066, 499 18685, 9990, 1257, 0
Average	Original Enhanced	14177, 5525, 1260, 73 11139, 2780, 176, 0

TABLE V
RESULTS FOR 4×12 MIMO (QPSK)

Transducer Index	Equ. Algorithm	Err. Num. ($1 \sim 5$ Iter.)
1	Original Enhanced	3469, 1205, 198, 0, 0 3012, 508, 9, 0, 0
2	Original Enhanced	5736, 3689, 1070, 38, 0 5196, 1937, 84, 0, 0
3	Original Enhanced	9147, 7735, 3985, 153, 2 8224, 5229, 284, 0, 0
4	Original Enhanced	5040, 2037, 411, 13, 0 3301, 830, 16, 0, 0
Average	Original Enhanced	5848, 3667, 1416, 51, 1 4933, 2126, 98, 0, 0

VII. Conclusion

An enhanced MIMO LMMSE turbo equalization scheme was proposed in this paper. The new equalization performed hybrid SOIC by incorporating both the *a priori* soft decisions and the *a posteriori* soft decisions of the interfering symbols. The hybrid SOIC led to extra performance gains over the conventional SOIC using only the *a priori* soft decisions. A novel block-wise reliability-based ordering scheme was then proposed to reduce error propagation, thus improved the performance of HSOIC. The new ordering scheme required only the symbol *a priori* information which was obtained at a very small overhead. Moreover, it enabled a dynamic 2-D space-time ordering which was unavailable with existing ordering schemes. To meet the practical needs, a low-complexity implementation of the enhanced turbo equalization was also provided. Different from most low-complexity implementations with constant equalizer taps, the proposed low-complexity solution allowed the equalizer taps to be flexibly updated during the equalization process, enabling a tradeoff between the tap updating complexity and the detection performance. The performance of the proposed MIMO LMMSE turbo equalization has been verified by both computer simulations and real-world undersea experimental results.

Acknowledgment

The authors would like to thank Dr. J. Preisig and his team for conducting the SPACE08 experiment.

References

[1] L. Bahl, J. Cocke, F. Jelinek, and J. Raviv, "Optimal decoding of linear codes for minimizing symbol error rate," *IEEE Trans. Inf. Theory*, vol. 20, no. 2, pp. 284–287, Mar. 1974.

[2] C. Douillard, M. Jezequel, C. Berrou, A. Picart, P. Didier, and A. Glavieux, "Iterative correction of intersymbol interference: turbo-equalization," *Eur. Trans. Telecommun.*, vol. 6, pp. 507–511, Sep. 1995.

[3] J. Hagenauer and P. Hoher, "A Viterbi algorithm with soft-decision outputs and its applications," in *Proc. IEEE GLOBECOM*, Nov. 1989, pp. 1680–1686.

[4] F. K. H. Lee and P. J. Mclane, "Parallel-trellis turbo equalizers for sparse-coded transmission over SISO and MIMO sparse multipath channels," *IEEE Trans. Wireless Commun.*, vol. 5, no. 12, pp. 3568–3578, Dec. 2006.

[5] J. Tao, Y. R. Zheng, C. Xiao, T. C. Yang, and W. B. Yang, "Channel equalization for single carrier MIMO underwater acoustic communications," *EURASIP J. Adv. Signal Process.*, vol. 2010, 2010, Article ID 281769, 17 pages.

[6] X. Wang and H. V. Poor, "Iterative (turbo) soft interference cancellation and decoding for coded CDMA," *IEEE Trans. Commun.*, vol. 47, no. 7, pp. 1046–1061, Jul. 1999.

[7] Z. Wu and J. Cioffi, "Low complexity iterative decoding with decision-aided equalization for magnetic recording channels," *IEEE J. Sel. Areas Commun.*, vol. 19, no. 4, pp. 699–708, Apr. 2001.

[8] C. Laot, A. Glavieux, and J. Labat, "Turbo equalization: Adaptive equalization and channel decoding jointly optimized," *IEEE J. Sel. Areas Commun.*, vol. 19, no. 9, pp. 1744–1752, Sep. 2001.

[9] M. Tüchler, A. C. Singer, and R. Koetter, "Minimum mean square error equalization using *a priori* information," *IEEE Trans. Signal Process.*, vol. 50, no. 3, pp. 673–683, Mar. 2002.

[10] R. Koetter, A. C. Singer, and M. Tüchler, "Turbo equalization," *IEEE Signal Process. Mag.*, vol. 21, no. 1, pp. 67–80, Jan. 2004.

[11] S. Jiang, L. Ping, H. Sun, and C. S. Leung, "Modified LMMSE turbo equalization," *IEEE Commun. Lett.*, vol. 8, no. 3, pp. 174–176, Mar. 2004.

[12] C. Laot, R. L. Bidan, and D. Leroux, "Low complexity MMSE turbo equalization: A possible solution for edge," *IEEE Trans. Wireless Commun.*, vol. 4, no. 3, pp. 965–974, May 2005.

[13] T. Abe and T. Matsumoto, "Space-time turbo equalization in frequency selective MIMO channels," *IEEE Trans. Veh. Technol.*, vol. 52, no. 3, pp. 469–475, May 2003.

[14] R. Visoz, A. O. Berthet, and S. Chtourou, "A new class of iterative equalizers for space-time BICM over MIMO block fading multi-path AWGN channel," *IEEE Trans. Commun.*, vol. 53, no. 12, pp. 2076–2091, Dec. 2005.

[15] G. Bauch and N. Al-dhahir, "Reduced-complexity space-time turbo-equalization for frequency-selective MIMO channels," *IEEE Trans. Wireless Commun.*, vol. 1, no. 4, pp. 819–828, Oct. 2002.

[16] Y. Sun, V. Tripathi, and M. L. Honig, "Adaptive turbo reduced-rank equalization for MIMO channels," *IEEE Trans. Wireless Commnun.*, vol. 4, no. 6, pp. 2789–2800, Nov. 2005.

[17] R. R. Lopes and J. R. Barry, "The soft-feedback equalizer for turbo equalization of highly dispersive channels," *IEEE Trans. Commun.*, vol. 54, no. 5, pp. 783–788, May 2006.

[18] S. Roy, T. M. Duman, V. McDonald, and J. G. Proakis, "High-rate communication for underwater acoustic channels using multiple transmitters and space-time coding: receiver structures and experimental results," *IEEE J. Ocean. Eng.*, vol. 32, no. 3, pp. 663–688, Jul. 2007.

[19] J. Wu and Y. R. Zheng, "Low complexity soft-input soft-output block decision feedback equalization," *IEEE J. Sel. Areas Commun.*, vol. 26, no. 2, pp. 281–289, Feb. 2008.

[20] J. Tao, J. Wu, and Y. R. Zheng, "Low-complexity turbo block decision feedback equalization for MIMO systems," in *Proc. IEEE Int. Conf. Commun.*, May 2010, pp. 1–5.

[21] G. K. Kaleh, "Channel equalization for block transmission systems," *IEEE J. Sel. Areas Commun.*, vol. 13, no. 1, pp. 110–121, Jan. 1995.

[22] J. M. Cioffi and G. D. Forney, "Generalized decision-feedback equalization for packet transmission with ISI and Gaussian noise," in *Communications, Computation, Control and Signal Processing: A Tribute to Thomas Kailath*, A. Paulraj, V. Roychowdhury, and C. D. Shaper, Eds. Norwell, MA: Kluwer, 1997.

[23] P. Schniter, "Low-complexity equalization of OFDM in doubly selective channels," *IEEE Trans. Signal Process.*, vol. 52, no. 4, pp. 1002–1011, Apr. 2004.

[24] P. W. Wolniansky, G. J. Foschini, G. D. Golden, and R. A. Valenzuela, "V-BLAST: An architecture for realizing very high data rates over the rich-scattering wireless channel," presented at the ISSSE, Pisa, Italy, Sep. 1998.

[25] A. Lozano and C. Papadias, "Layered space-time receivers for frequency-selective wireless channels," *IEEE Trans. Commun.*, vol. 50, no. 1, pp. 65–73, Jan. 2002.

[26] S. W. Kim and K. P. Kim, "Log-likelihood-ratio-based detection ordering in V-BLAST," *IEEE Trans. Commun.*, vol. 54, no. 2, pp. 302–307, Feb. 2006.

Jun Tao (S'10–M'10) received the B.S. and M.S. degrees in electrical engineering from the Department of Radio Engineering, Southeast University, Nanjing, China, in 2001 and 2004, respectively, and the Ph.D. degree in electrical engineering from the Department of Electrical and Computer Engineering, University of Missouri, Columbia, in 2010.

From 2004 to 2006, he was a System Design Engineer with Realsil Microelectronics, Inc. (a subsidiary of Realtek), Suzhou, China. He is currently a Postdoctoral Fellow at the Department of Electrical and Computer Engineering, Missouri University of Science and Technology, Rolla. His research interests include channel modeling, channel estimation, and turbo equalization for wireless radio-frequency communications, and robust signal detection for underwater acoustic communications. He is the holder of one IC chip design patent, which has been commercialized.

Jingxian Wu (S'02–M'06) received the B.S. degree in electronic engineering from Beijing University of Aeronautics and Astronautics, Beijing, China, in 1998, the M.S. degree in electronic engineering from Tsinghua University, Beijing, China, in 2001, and the Ph.D. degree in electrical engineering from the University of Missouri, Columbia, in 2005.

He is currently an Assistant Professor with the Department of Electrical Engineering, University of Arkansas, Fayetteville. His research interests mainly focus on wireless communications and wireless networks, including ultra-low power communications, cooperative communications, cognitive radio, and cross-layer optimization, etc.

Dr. Wu is currently an Associate Editor of the IEEE TRANSACTIONS ON VEHICULAR TECHNOLOGY. He served as a Co-Chair for the 2012 Wireless Communication Symposium of the IEEE International Conference on Communication, and a Co-Chair for the 2009 Wireless Communication Symposium of the IEEE Global Telecommunications Conference. Since 2006, he has served as a Technical Program Committee Member for a number of international conferences, including the IEEE Global Telecommunications Conference, the IEEE Wireless Communications and Networking Conference, the IEEE Vehicular Technology Conference, and the IEEE International Conference on Communications.

Yahong Rosa Zheng (S'99–M'03–SM'07) received the B.S. degree from the University of Electronic Science and Technology of China, Chengdu, China, in 1987, the M.S. degree from Tsinghua University, Beijing, China, in 1989, both in electrical engineering, and the Ph.D. degree from the Department of Systems and Computer Engineering, Carleton University, Ottawa, Canada, in 2002.

She was an NSERC Postdoctoral Fellow from 2003 to 2005 at the University of Missouri-Columbia. Since 2005, she has been a faculty member with the Department of Electrical and Computer Engineering at the Missouri University of Science and Technology. Her research interests include array signal processing, wireless communications, and wireless sensor networks.

Dr. Zheng has served as a Technical Program Committee (TPC) member for many IEEE international conferences, including VTC, Globecom, ICC, WCNC, and Aerospace Conference. She served as an Associate Editor for the IEEE TRANSACTIONS ON WIRELESS COMMUNICATIONS from 2006 to 2008. She was the recipient of an NSF CAREER award in 2009.

Chengshan Xiao (M'99–SM'02–F'10) received the B.S. degree in electronic engineering from the University of Electronic Science and Technology of China, Chengdu, China, in 1987, the M.S. degree in electronic engineering from Tsinghua University, Beijing, China, in 1989, and the Ph.D. degree in electrical engineering from the University of Sydney, Sydney, Australia, in 1997.

From 1989 to 1993, he was with the Department of Electronic Engineering, Tsinghua University, where he was a Research Staff and then a Lecturer. From 1997 to 1999, he was a Senior Member of Scientific Staff with Nortel, Ottawa, ON, Canada. From 1999 to 2000, he was a Faculty Member with the University of Alberta, Edmonton, AB, Canada. From 2000 to 2007, he was with the University of Missouri, Columbia, where he was an Assistant Professor and then an Associate Professor. He is currently a Professor with the Department of Electrical and Computer Engineering, Missouri University of Science and Technology, Rolla (formerly University of Missouri, Rolla). His research interests include wireless communications, signal processing, and underwater acoustic communications. He is the holder of three U.S. patents. His algorithms have been implemented into Nortel's base station radios after successful technical field trials and network integration.

Dr. Xiao is the Editor-in-Chief of the IEEE TRANSACTIONS ON WIRELESS COMMUNICATIONS, a Distinguished Lecturer of the IEEE Communications Society, and a Fellow of the IEEE. Previously, he served as the founding Area Editor for Transmission Technology of the IEEE TRANSACTIONS ON WIRELESS COMMUNICATIONS; an Associate Editor of the IEEE TRANSACTIONS ON VEHICULAR TECHNOLOGY, the IEEE TRANSACTIONS ON CIRCUITS AND SYSTEMS I, and the international journal of *Multidimensional Systems and Signal Processing*. He was the Technical Program Chair of the 2010 IEEE International Conference on Communications (ICC), the Lead Co-Chair of the 2008 IEEE ICC Wireless Communications Symposium, and a Phy/MAC Program Co-Chair of the 2007 IEEE Wireless Communications and Networking Conference. He served as the founding Chair of the IEEE Technical Committee on Wireless Communications, and the Vice-Chair of the IEEE Technical Committee on Personal Communications.